AIP Advances

Infrared transparent frequency selective surface based on metallic meshes

Miao Yu, Nianxi Xu, Hai Liu, and Jinsong Gao

Citation: AIP Advances **4**, 027112 (2014); doi: 10.1063/1.4866292
View online: http://dx.doi.org/10.1063/1.4866292
View Table of Contents: http://scitation.aip.org/content/aip/journal/adva/4/2?ver=pdfcov
Published by the AIP Publishing

AIP ADVANCES **4**, 027112 (2014)

Infrared transparent frequency selective surface based on metallic meshes

Miao Yu,[1,2] Nianxi Xu,[1] Hai Liu,[1] and Jinsong Gao[1,a]
[1]*Key Laboratory of Optical System Advanced Manufacturing Technology, Changchun Institute of Optics, Fine Mechanics and Physics, Chinese Academy of Sciences, Changchun, 130033, China*
[2]*University of Chinese Academy of Sciences, Beijing, 100049, China*

(Received 19 December 2013; accepted 7 February 2014; published online 14 February 2014)

This paper presents an infrared transparent frequency selective surface (ITFSS) based on metallic meshes. In this ITFSS structure, periodic cross-slot units are integrated on square metallic meshes empowered by coating and UV-lithography. A matching condition is proposed to avoid the distortion of units. Experimental results show that this ITFSS possesses a good transmittance of 80% in the infrared band of 3–5 μm, and also a stable band-pass behavior at the resonance frequency of 36.4 GHz with transmittance of −0.56 dB. Theoretical simulations about the ITFSS diffractive characteristics and frequency responses are also investigated. The novel ITFSS will attract renewed interest and be exploited for applications in various fields. [http://dx.doi.org/10.1063/1.4866292]

I. INTRODUCTION

Frequency selective surface (FSS) consists of two-dimensional array of metallic patches or apertures in a thin conducting film and has been widely used as a filter in microwave and millimeter wave band.[1–3] To improve the filtering effect, the metal with high conductivity is always adopted in the classical FSS fabrication process, such as copper, aluminum or silver. However, the utilization of the metal raises a problem that the FSS has a low transmittance in the optical band (from ultraviolet to infrared), which limits its applications in several fields, e.g., the energy saving window panels,[4] the wall for securing indoor wireless networks[5] and the dome on the aircrafts. Especially for the application on the dome, the FSS should have a high transmittance in the infrared band of 3–5 μm for imaging sensor and also a band-pass filtering effect in the Ka-band (26–40 GHz) for receiving radar signals.[6] Although the optically transparent FSS has been developed by different methods,[7,8] the transparent range is only focused in the visible spectrum which is not suitable for the dome application. Therefore, an infrared transparent frequency selective surface (ITFSS) needs to be developed to broaden the application fields of FSS.

In this paper, a novel ITFSS which is transparent at infrared wavelength and band-pass in millimeter wave band is reported. On the basis of the coating and UV-lithography technology, periodic cross-slot units are integrated on the square metallic meshes to form the ITFSS structure, followed by a matching condition to keep the integrity of units. Experimentally, the ITFSS possesses the transmittances of 80% in the infrared band of 3–5 μm and −0.56 dB at the resonance frequency of 36.4 GHz, respectively. Theoretical simulations about the ITFSS characteristics show that the ITFSS can suppress the stray light effectively to improve the infrared imaging quality and have a stable band-pass effect which is insensitive to the incident angle of millimeter wave. This work provides impetus towards the development of ITFSS and its practical applications.

[a]Author to whom correspondence should be addressed. Electronic mail: gaojs@ciomp.ac.cn

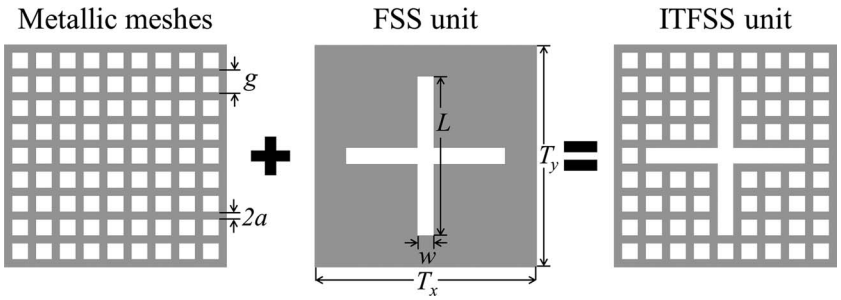

FIG. 1. Schematic diagram of ITFSS unit.

II. ITFSS STRUCTURE AND FABRICATION

Fig. 1 shows the schematic diagram of the proposed ITFSS unit, which is composed of square metallic meshes and cross-slot FSS unit (the shadow part is metal). The metallic meshes can provide high transmittance in the infrared band but lack of frequency selective capability in the millimeter wave band,[9,10] which is just opposite to the typical FSS. We hope to combine these advantages by integration of the two structures. The metallic meshes have the period g and linewidth $2a$. In a FSS unit, the cross-slot with width w and length L is etched on a metal plate with unit period T_x and T_y along two directions. To avoid the distortion of units in the integration process which will lead to a shift of resonance frequency, a matching condition is proposed and expressed by the following equations:

$$w = k \times g - 2a, \tag{1}$$

$$L = m \times g - 2a, \tag{2}$$

$$T_x = T_y = n \times g, \tag{3}$$

where k, m and n are the positive integers used to control the position and size of FSS unit in the metallic meshes. Taking the ITFSS unit shown in Fig. 1 as an example, k, m and n are equal to 1, 7 and 9, respectively.

The fabrication procedure of the ITFSS by coating and UV-lithography is as follows: 1) the photoresist is deposited on a MgF_2 substrate ($\varepsilon_r = 4.8$) with a thickness of 3.82 mm; 2) a chromium (Cr) plate is used as a mask for UV-lithography; 3) after exposure, a copper (Cu, $\sigma = 59.6 \times 10^6$ S/m) film with a thickness of 0.8 μm is deposited on the processed substrate; 4) an ITFSS sample is obtained after stripping the residual photoresist. The parameters chosen in our experiment are summarized as follows: $g = 350$ μm, $2a = 15$ μm, $T_x = T_y = 3.15$ mm, $w = 0.335$ mm, $L = 2.435$ mm and the overall size of the ITFSS sample is about 70 mm $\times$ 70 mm. The ITFSS unit is designed for a resonance frequency of 37 GHz which is of great interest in our experiment. A micrograph of the ITFSS sample under a 300$\times$ optical microscope (MF-B3017B, Mitutoyo Corporation) is shown in Fig. 2, in which the white line is copper.

III. ITFSS CHARACTERISTICS IN INFRARED BAND

A. Transmittance characteristics

On the basis of the scalar diffraction analysis, the transmittance of ITFSS in infrared band can be estimated by its obscuration ratio, which is used to indicate the fraction of the area without metal.[11] According to the structure shown in Fig. 1, the transmittance of ITFSS can be expressed by:

$$T_{\mathrm{ITFSS}} = \left(1 - \frac{2a}{g}\right)^2 \left(1 - \frac{2km - k^2}{n^2}\right) + \frac{2km - k^2}{n^2} + \frac{4a^2 - 4amg}{n^2 g^2}. \tag{4}$$

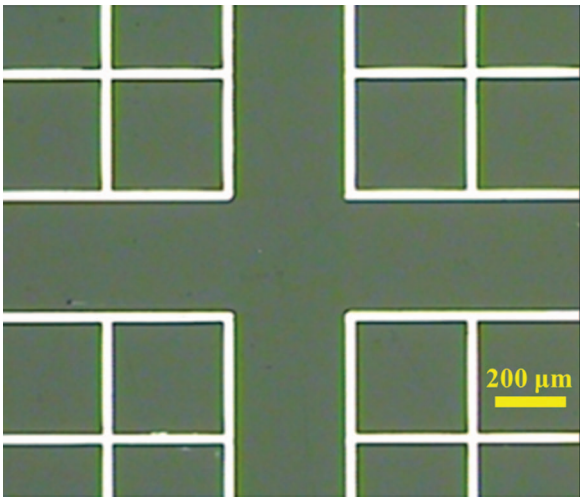

FIG. 2. Micrograph of ITFSS sample.

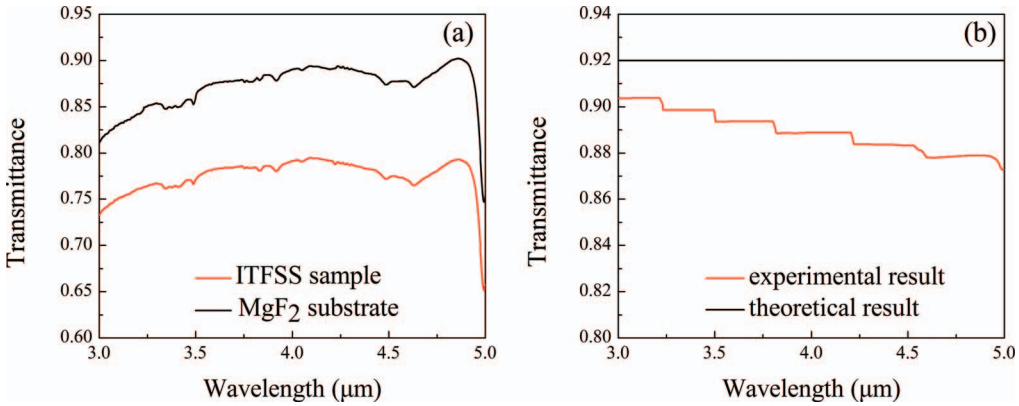

FIG. 3. (a) Transmittances of ITFSS sample and MgF_2 substrate and (b) comparison between experimental and theoretical results for transmittance of separate ITFSS.

For the ITFSS sample fabricated in Section II, its transmittance is calculated using Eq. (4) as about 92%. To verify the validity of the theoretical result, a Fourier transform infrared spectrometer (Spectrum Gx, Perkin Elmer Corporation) is used to measure the transmittance in the infrared band of 3–5 μm. It can be seen from Fig. 3(a) that the ITFSS sample has an average transmittance of 76% in the infrared band, and the maximum up to 80% is obtained. The transmittance of MgF_2 substrate is also measured and used to obtain the transmittance of separate ITFSS structure without substrate, according to the ratio of ITFSS sample to MgF_2 substrate. The calculated results are shown in Fig. 3(b). The separate ITFSS structure possesses an average transmittance of 89%, which has a good agreement with the theoretical results of 92%. Moreover, the transmittance of separate ITFSS structure as a function of relative linewidth ($2a/g$) is simulated, as shown in Fig. 4. With the increasing relative linewidth, the transmittance decreases because of the reduction of the obscuration ratio. It can be found that an ITFSS sample with higher transmittance will be achieved by selecting more transparent substrate and lowering the relative linewidth.

B. Diffractive characteristics

When illuminated by the infrared wave, the ITFSS will act as a two-dimensional diffraction grating and produce diffractive orders. For an imaging system, only the zero-order diffraction is of interest and the higher-order diffractive light degrades the imaging quality as undesirable stray light.

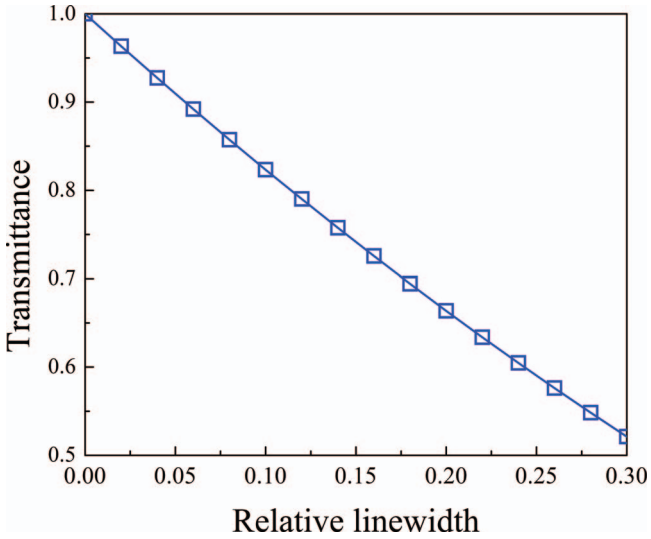

FIG. 4. Transmittance of separate ITFSS as a function of relative linewidth.

Therefore, the diffractive characteristics of the ITFSS are analyzed theoretically compared to the square metallic meshes which have been widely used in infrared system.[11,12] The Fourier diffraction theory is used here to obtain the diffractive characteristics of the ITFSS and the square metallic meshes. The distribution of diffractive light intensity is given by the modulus squared of the Fourier transform of the pupil function.[13] The pupil functions of square metallic meshes and ITFSS can be expressed by:

$$t_{\text{meshes}}(x, y) = [rect\left(\frac{x}{g-2a}\right) rect\left(\frac{y}{g-2a}\right) \otimes \sum_{p=-\infty}^{\infty} \delta(x-pg) \otimes \sum_{q=-\infty}^{\infty} \delta(x-qg)] \times rect\left(\frac{x}{Mg}, \frac{y}{Mg}\right), \tag{5}$$

$$\begin{aligned} t_{\text{ITFSS}}(x, y) = \{[t_{\text{meshes}}(x, y) \times & \left(1 - rect\left(\frac{x}{w}\right) rect\left(\frac{y}{L}\right) - rect\left(\frac{x}{L}\right) rect\left(\frac{y}{w}\right) + rect\left(\frac{x}{w}\right) rect\left(\frac{y}{w}\right)\right) \\ & + rect\left(\frac{x}{w}\right) rect\left(\frac{y}{L}\right) + rect\left(\frac{x}{L}\right) rect\left(\frac{y}{w}\right) - rect\left(\frac{x}{w}\right) rect\left(\frac{y}{w}\right)] \\ & \otimes \sum_{p=-\infty}^{\infty} \delta(x - pT_x) \otimes \sum_{q=-\infty}^{\infty} \delta(y - qT_y)\} \\ & \times rect\left(\frac{x}{NT_x}, \frac{y}{NT_y}\right) \end{aligned} \tag{6}$$

where p and q are integers, and M and N are the sizes of square metallic meshes and ITFSS, respectively.

Based on the Eqs. (5) and (6), the diffractive light intensity distributions of ITFSS and square metallic meshes with equivalent parameters are simulated and shown in Fig. 5. The incident infrared wavelength is fixed at 3 μm. It can be clearly seen that the higher-order diffractive light concentrates along the two axes for both structures. However, the higher-order diffractive light intensity of ITFSS is much lower than the one of square metallic meshes, which indicates that the ITFSS produces less stray light. The theoretical simulations show that the ITFSS structure has the capability to suppress the stray light effectively, and thus improve the infrared imaging quality.

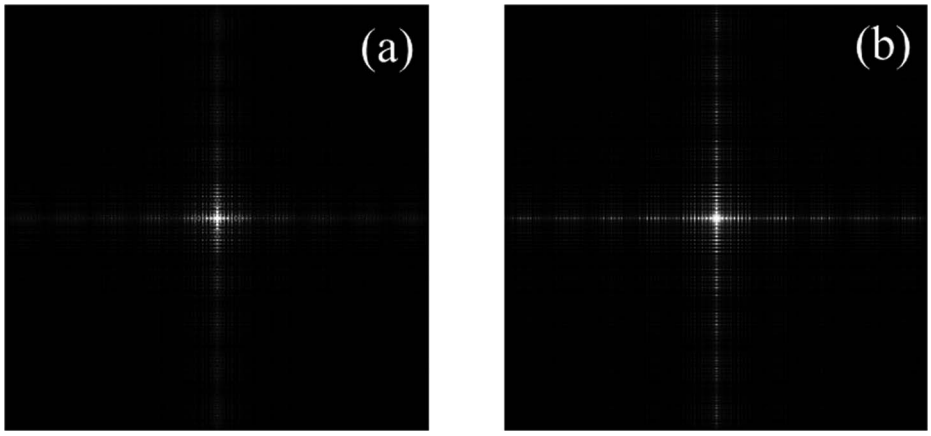

FIG. 5. Comparison of diffractive light intensity distributions between (a) ITFSS and (b) square metallic meshes.

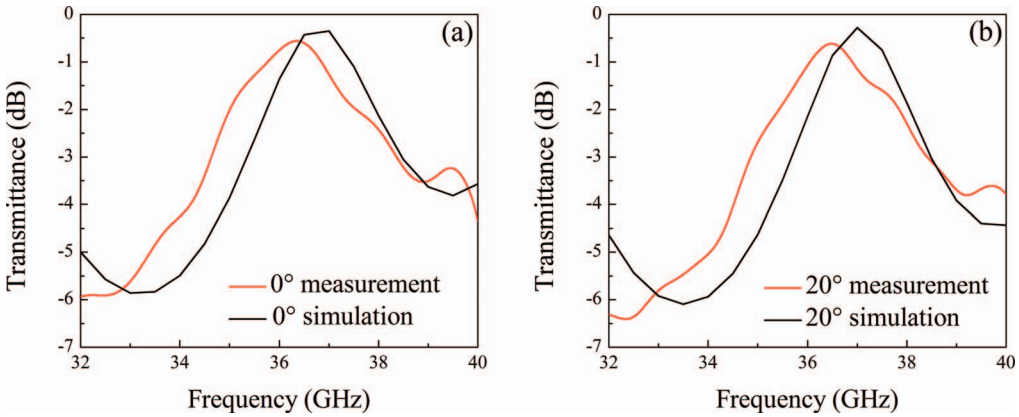

FIG. 6. Comparison of transmittance responses between the measurement and simulation results with (a) 0° and (b) 20° incident angles.

IV. ITFSS CHARACTERISTICS IN MILLIMETER WAVE BAND

To measure the transmittance response of the ITFSS in millimeter wave band, the ITFSS sample is mounted on a bench between two lens antennas connected to the network analyzer (Aglient N5244A) in dark room. Fig. 6 shows the measured transmittance responses for TE wave with different incident angles. For the normal incident wave, a band-pass effect at the resonance frequency of 36.4 GHz with the transmittance of −0.56 dB is achieved, and the −3 dB bandwidth is about 3.6 GHz. As the incident angle increases to 20°, the resonance frequency shifts to 36.5 GHz, the transmittance decreases to −0.61 dB but the −3 dB bandwidth remains the same. It is therefore concluded that the ITFSS possesses a stable band-pass behavior for its insensitivity to the incident angle. The theoretical simulations using the periodic method of moments[14,15] for different incident angles are also plotted in Fig. 6. Compared to the simulation results, a slightly shift of resonance frequency about 0.4 GHz is found in the measurement which may attribute to the processing errors of ITFSS sample. The good agreement between measurements and simulation results indicates that the ITFSS sample can be designed or optimized. To further improve the transmittance of the ITFSS at the resonance frequency, we should increase the conductance of the ITFSS structure.[16] An effective method is to increase the linewidth $2a$ to introduce more copper into this structure. However, as mentioned in Section III, the higher linewidth will decrease the transmittance of the ITFSS in the infrared band. Therefore, a trade-off between the infrared transmittance and the transmittance response in millimeter wave band should be considered for specific application requirements. The optimization work of this ITFSS is undergoing.

V. CONCLUSIONS

In conclusion, a novel ITFSS based on metallic meshes empowered by coating and UV-lithography has been successfully demonstrated. In this ITFSS structure, periodic cross-slot FSS units are integrated on square metallic meshes and a matching condition is proposed to avoid the distortion of units. In the infrared band of 3–5 μm, a transmittance of 80% is obtained from the ITFSS with the MgF_2 substrate. Comparative simulations with square metallic meshes show that the ITFSS has a better infrared imaging quality because it can suppress the stray light effectively. In the millimeter wave band, the ITFSS has a band-pass behavior at the resonance frequency of 36.4 GHz with transmittance of −0.56 dB. Measurement and simulation results both prove that the band-pass effect is stable for its insensitivity to the incident angle. The good performance of the novel ITFSS in the infrared and millimeter wave bands will benefit its practical applications.

ACKNOWLEDGMENTS

This work is funded by the National Natural Science Foundation of China (Grant No. 61172012), and the Third Innovation of Changchun Institute of Optics, Fine Mechanics and Physics, Chinese Academy of Sciences (Grant No. 093Y32J090).

[1] R. Mittra, C. H. Chan, and T. Cwik, P. IEEE. **76**, 1593 (1988).
[2] T. K. Wu, *Frequency selective surface and grid array* (Wiley-Interscience, 1995).
[3] B. Li and Z. Shen, Appl. Phys. Lett. **103**, 171607 (2013).
[4] G. I. Kiani, L. G. Olsson, A. Karlsson, K. P. Esselle, and M. Nilsson, IEEE. T. Antenn. Propag. **59**, 520 (2011).
[5] D. J. Kozakoff, *Analysis of radome-enclosed antennas* (Artech House, 2010).
[6] M. Salehi and N. Behdad, IEEE. Microw. Wirel. Co. **18**, 785 (2008).
[7] E. A. Parker, C. Antonopoulos, and N. E. Simpson, Microw. Opt. Techn. Let. **16**, 61 (1997).
[8] C. Tsakonas, S. C. Liew, C. Mias, D. C. Koutsogeorgis, R. M. Ranson, W. M. Cranton, and M. Dudhia, Electron. Lett. **37**, 1464 (2001).
[9] O. Limaj, S. Lupi, F. Mattioli, R. Leoni, and M. Ortolani, Appl. Phys. Lett. **98**, (2011).
[10] S. Gupta, G. Tuttle, M. Sigalas, and K. Ho, Appl. Phys. Lett. **71**, 2412 (1997).
[11] M. Kohin, S. J. Wein, J. D. Traylor, R. C. Chase, and J. E. Chapman, Opt. Eng. **32**, 911 (1993).
[12] J. Tan and Z. Lu, Opt. Express **21**, 790 (2007).
[13] J. W. Goodman, *Introduction to Fourier optics* (Roberts and Company Publishers, 2005).
[14] B. Monacelli, J. B. Pryor, B. A. Munk, D. Kotter, and G. D. Boreman, IEEE. T. Antenn. Propag. **53**, 745 (2005).
[15] X. Dardenne and C. Craeye, IEEE. T. Antenn. Propag. **56**, 2372 (2008).
[16] M. Gustafsson, A. Karlsson, A. P.P. Rebelo, and B. Widenberg, IEEE. T. Antenn. Propag. **54**, 1897 (2006).